ACS OMEGA

Open Access

http://pubs.acs.org/journal/acsodf

Article

Diterpenoid Tanshinones Can Inhibit Lung Cancer Progression by Improving the Tumor Microenvironment and Downregulation of NF-κB Expression

Hao Xu,[⊥] Ning Ning Guo,[⊥] Chen Ying Zhu, Lin Yan Ye, Xing Yi Yan, Yong Qin Liu, Ze Yan Zhang, Guangji Zhang,* and Liaqat Hussain*

Cite This: *ACS Omega* 2024, 9, 7230−7238

Read Online

ACCESS | Metrics & More | Article Recommendations

ABSTRACT: Diterpenoid tanshinones (DTs) are a bioactive fraction extracted from *Salvia miltiorrhiza*. High-performance liquid chromatography analysis revealed the presence of four compounds, namely, tanshinone IIA, tanshinone I, cryptotanshinone, and dihydrotanshinone. In this study, we aimed to propose a possible mechanism for the anti-lung cancer effect of DT. To do so, we utilized a lung cancer nude mice model and a lung cancer cell line (PC9) to investigate the effect of DT on lung cancer. We employed immunohistochemistry, enzyme-linked immunosorbent assay, hematoxylin and eosin staining, and immunofluorescence to analyze the pharmacological role of DT in the inhibition of lung cancer growth. The results showed that DT inhibited tumor growth, induced apoptosis in the nude mice model, and reduced inflammatory cell infiltration. Additionally, DT inhibited PC9 lung cancer cells, growth, proliferation, and migration. The mechanism of action of DT involves not only directly inhibiting cell proliferation and migration but also improving the tumor microenvironment. DT significantly increased the expression of important intestinal gap junction proteins, such as zonula occludens 1 (ZO-1) and occludin I. This upregulation contributes to the reinforcement of the intestinal mucosal barrier, thereby reducing the paracellular transport of lipopolysaccharides (LPS) through the intestine. Consequently, the decreased LPS levels lead to the inhibition of NF-κB expression and downregulation of macrophage polarization, as indicated by the decreased expression of CD68. In conclusion, this study has confirmed that DT has anti-lung cancer properties by improving the inflammatory tumor microenvironment via regulating macrophage polarization and inhibiting LPS-associated immune response. These results provide new insights into the mechanism of DT action against lung cancer.

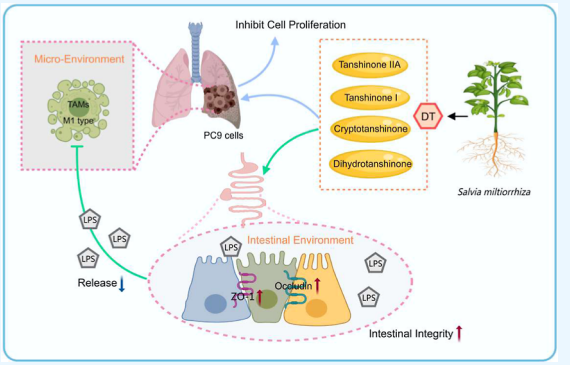

1. INTRODUCTION

Lung cancer is the leading cause of cancer-related death with a high incidence of mortality. The latest data showed the total number of diagnosed lung and bronchioles cancer cases was 221,097 in the United States in 2019, with a death count of 13,960.[1] It is predicted that 238,340 adults (117,550 men and 120,790 women) will be diagnosed with lung cancer in 2023 in the United States.[2] Lung cancer is characterized by high malignancy, rapid progression, early metastasis, poor prognosis, and frequent recurrence. Lung cancer treatments have been diversified and innovated over time. Recently, several treatment options have become available to lung cancer patients. These include chemotherapy, immunotherapy, targeted therapies using monoclonal antibodies, and various combinatorial and adjuvant therapies.[3] However, due to the quick progression and poor prognosis of lung cancer, researchers are continuously working to identify novel modalities for curing this disease.

Salvia miltiorrhiza is a traditional Chinese medicine that has been used for treating cerebrovascular and cardiovascular ailments for many years. It has recently gained attention due to its bioactive component, which is rich in tanshinones, a group of natural compounds containing an anthraquinone ring.[4] Research is ongoing to investigate the anticancer potential of this bioactive fraction. This bioactive fraction mostly contains tanshinone IIA, tanshinone I, cryptotanshinone, and dihydrotanshinone.[4−7] Tanshinone IIA has been shown to inhibit colon cancer cell growth.[8] Tanshinone I blocks ovarian cancer proliferation,[9] and cryptotanshinone inhibits the proliferation

Received: December 4, 2023
Revised: January 10, 2024
Accepted: January 23, 2024
Published: February 2, 2024

of cancer cells.[10] Anthraquinones in traditional Chinese medicine often have sound anticancer effects, including *Aloe rhodopsin*[11] and norethindrone.[12]

Our previous studies[13−16] revealed that tanshinone IIA alone and in combination with cisplatin decreased the mitochondrial membrane potential of human lung adenocarcinoma PC9 cells in a concentration-dependent manner, upregulated the amount of intracellular reactive oxygen species, and promoted apoptosis in lung cancer cells. Tanshinone IIA also significantly inhibited the proliferation, migration, and invasion of PC9 lung cancer cells by regulating the coagulation-related factors of the transmembrane glycoprotein mucin 1 (MUC1), p-selectin glycoprotein ligand-1 (PSGL-1), and tissue factor and impacting the phosphoinositide 3-kinase/protein kinase B (PI3K/Akt) signaling pathway. Moreover, researchers have found that tanshinone IIA inhibited tumor cell growth and proliferation, tumor cell invasion and migration, tumor angiogenesis, and induced tumor cell autophagy.[4] Cryptotanshinone has been found to have an anticancer effect by regulating NF-κB, MAPK, JAK, and STAT4 signals in immune-related cells, such as macrophages, NK cells, CD4 cytotoxic (CT) cells, and dendritic cells.[17] On the other hand, tanshinone I has been reported to induce apoptosis in cancer cells by regulating the cell cycle and to inhibit the invasion and migration of cancer cells by suppressing the MMP-2 and MMP-9 signaling pathways.[18]

The tumor microenvironment (TME) plays a crucial role in tumorigenesis. The TME contains tumor cells that interact with the surrounding medium through the circulatory and lymphatic systems, leading to the progression of cancer cells. The TME comprises various cellular components, such as vascular endothelial cells, immune cells (macrophages), and extracellular matrix. Therefore, improving the TME is a vital determinant of tumor growth, progression, and prognosis. TME improvement can be assessed by downregulating various protein markers such as CD31, CD38, and others.[19] Tumor-associated macrophages (TAMs) are polarized into M1 and M2 phenotypes. The inflammatory response mediated by M1 phenotype macrophages has been shown to promote the ability of tumor cells to invade and metastasize[20,21] thus provoking a malignant cycle of "inflammation-cancer" transformation. M2 phenotype macrophages may play a more benign role in regulating the inflammatory microenvironment of tumors due to their immunosuppressive characteristics.[22] Among the various stimulators, lipopolysaccharide (LPS) induces macrophage M1 polarization.[23] However, the relationship between LPS and lung cancer still needs more understanding. Intestinal damage induces LPS through multiple pathways.[24,25] A few recent studies investigated possible links between the intestinal microenvironment and the pathogenesis of various cancers.[26−28] Inflammation of the lung and intestine can trigger changes in the gut microenvironment, thereby initiating the development of cancer.[29] In this study, our objective was to investigate the mechanism behind the anti-lung cancer activity of diterpenoid tanshinone (DT) and to explore the potential downregulation of LPS-TLR4-NFκB expression in improving the TME.

2. MATERIALS AND METHODS

2.1. DT Extraction. We used CO_2 supercritical fluid extraction on *S. miltiorrhiza*, where supercritical carbon dioxide and ethanol are used as cosolvents to extract the necessary components after crushing. The enriched extract comprised of the target component is collected and evaporated until completely dry for preparative separation. Further decompression recovery of the extract was carried out using countercurrent chromatography.[15] The resulting extract is initially dissolved in dimethyl sulfoxide to form a semifluid state and then diluted with 0.5% carboxymethyl cellulose sodium solution to create a semifluid DT-DMSO solution with a concentration of 100 mg/mL. The solution is stored in a sealed refrigerator at 4 °C in a dark environment. To use it, the stock solution was diluted with 0.5% carboxymethyl cellulose sodium, and three concentrations of drugs were prepared and placed in a 50 mL centrifuge tube. They should be stored in a refrigerator at 4 °C in the dark for future use and mixed well before use.

2.2. Preparation of the Tumor-Bearing Nude Mice Model. BALB/c-nu nude mice (3−5 weeks old males, $n = 70$) were purchased from the Animal Experiment Center, Zhejiang Chinese Medical University (ZCMU), and supplied by Shanghai Shrike animal production license number: SYXK (Zhejiang) 2018-0012. The institutional ethics approval number: IACUC-20200727-04 was obtained from the Animal Ethical and Welfare Committee of Zhejiang Chinese Medical University. Animals were divided into 5 groups; in each group, 10 animals were maintained. The animals were fed in SPF-level barrier animal rooms at the Animal Experiment Center of ZCMU. The temperature was maintained at 22 ± 1 °C and the humidity at 50−70%. All mice were fed for 1 week before the experiments, giving them free access to food and water.

The human lung cancer cell line PC9 was purchased from the cell bank of the Chinese Academy of Sciences (Shanghai, China). The cell lines were maintained in DMEM high-glucose medium (Biosharp, BL301A) containing 10% fetal bovine serum (FBS, Everspring Chemical, item no. 1101-8611) and 1% penicillin−streptomycin (Biosharp, BL505A) at 37 °C in a humidified atmosphere of 95% air and 5% CO_2. This was equivalent to the DMEM complete medium. PC9 cells were collected at the logarithmic growth stage, counted under the microscope, and then adjusted to a single-cell suspension with a density of 2×10^7/mL in PBS buffer. Cells were injected into the left axilla of drug-administered nude mice in a volume of 0.1 mL.[14,15] After inoculation, a cotton swab was used to gently press the site of the needle hole for 30 s to prevent leakage of the PC9 single-cell solution, with a distinct wound visible under the skin.

Water and food were administered normally during the tumor growth period. Various concentrations of DT (15, 30, and 60 mg/kg/day *p.o.*) were administered to three DT treatment groups by gavage, while physiological saline was given by injection. Paclitaxel group (PTX, 60 mg/kg/day, Aladdin L1910090) was administered by intraperitoneal injection (*i.p*), and physiological saline was given by gavage.

2.3. Hematoxylin and Eosin Staining. Tumor samples were fixed with 4% paraformaldehyde (PFA) solution for >48 h and then dehydrated, waxed, embedded, sliced, and dried in a 40 °C oven for 1 h. The sections were stained directly with a fully automated hematoxylin and eosin (H&E) staining machine (Gemini AS, Thermo Scientific) and sealed with neutral gum. Images were photographed with a Nikon Eclipse 80i Ti−S microscope.

2.4. Immunohistochemistry and Immunofluorescence Staining of Intestine and Tumor Tissue. Intestine and tumor samples were taken after routine dewaxing and hydration to transparency with deionized H_2O and Tris EDTA

https://doi.org/10.1021/acsomega.3c09667
ACS Omega 2024, 9, 7230−7238

(Biosharp, item BL617A) at a 49:1 volume ratio. After being soaked in 3% H_2O_2 for 5 min, the samples were blocked with QuickBlock blocking buffer for immunological staining (Beyotime, item no. P0260) at a volume ratio of 1:100−200. After incubation overnight in a 4 °C refrigerator, the samples were washed thoroughly with PBS, and the QuickBlock blocking buffer was added for immunological staining (Beyotime, item no. P0260) according to the source of the primary antibody species. The secondary antibody was added to the samples at a volume ratio of 7:1000 before incubation in the dark at 37 °C for 25−30 min. The samples were then washed thoroughly with PBS. For immunofluorescence, sections were sealed with a DAPI-containing blocking solution (Thermo Fisher, item no. P36966) and photographed with a Nikon Eclipse 80i Ti−S laser microscope. For immunohistochemistry (IHC), the samples were developed for 10−15 s with DAB chromogenic solution prepared with the DAB chromogenic kit (ZSGB-Bio, item no. ZLI9018), washed rapidly, and then re-stained in the Thermo Fisher automatic staining machine and sealed with neutral gum.[16]

The following antibodies were used: anti-CD31(Beyotime, item no. AF6408), anti-CD68 (Beyotime, item no. AF6432), anti-occludin 1 (Beyotime, item no. AF6504), anti-zonula occludens 1 (ZO-1) (Beyotime, item no. AF8394), anti-NF-κB (Beyotime, item no. AF1234), actin tracker red rhodamine (Beyotime, item no. C2207S), and Alexa Fluor 488 IgG (Beyotime, item no. A0423). Invitrogen ProLong Diamond Antifade Mountant solution was used with DAPI (Thermo Fisher, item no. P36966).

2.5. Cell Counting Kit-8 Detection of Cell Activity. PC9 cells were dispersed and subcultured with 0.25% trypsin-EDTA (Gibco 2120734) until the cells were in the logarithmic growth stage. Cells were counted microscopically and spread in 96-well plates (Corning, 3599) at 8000 cells/mL and 100 μL per well. 12 hours after the PC9 cells had reached a monolayer, the medium was discarded, and 100 μL per well of each DT concentration (1, 1.5, 2, 2.5, 5, 10, 20, and 40 μg/mL) diluted in DMEM complete medium was added. After 12 h, the medium was discarded, and 100 μL of the working solution prepared from the Cell Counting Kit-8 (CCK8) (MCE HY-K0301-3000T) and DMEM complete medium at 1:9 was added to each well and incubated for 30 min in a cell incubator (Thermo, 3111). The absorbance (OD) was detected by an enzyme marker (BioTek, ELX800) at 450 nm, and GraphPad calculated the IC_{50}.[16]

DT (0, 10, and 20 μg/mL) and PTX (10 μg/mL) were added as stimulus factors to PC9 96-well culture plates under the same plating conditions. These concentrations were chosen according to the IC_{50} and previously used conditions. Cell activity after 12 h of treatment was measured by the CCK8 method, and the efficacy of DT for cell inhibition was compared between samples.

2.6. Wound-Healing Assay and 8 μm Trans Well Assay of PC9 Cells. For wound-healing experiments, PC9 cells were counted microscopically and diluted to a concentration of 500,000 cells/mL, then seeded into 6-well plates (Corning 3516) at 1000 μL per well. Cells were grown for 12 h in a cell incubator until 90% confluence was reached and were then scratched with a sterile plastic tip. DT (0, 2.5, and 5 μg/mL) or PTX (1 μg/mL) was then added as stimulus factors, and the cells were cultured for 6 and 12 h with 10% FBS, DMEM. Furthermore, they were observed under a microscope (Nikon Ti−S) and photographed. For the trans well assay, 100 μL of PC9 cells at the logarithmic growth stage was cultured in a serum-free medium for 6 h and then added to the upper chamber of 8 μm 24 trans well plates (Corning, 3422) at a concentration of 5×10^4 cells/mL. Control, DT (2.5 μg/mL), DT (5 μg/mL), and PTX (1 μg/mL) groups were studied. The DMEM culture medium containing 10% serum was added to the lower chamber. Cells were then incubated for 12 h, the culture medium was discarded, and cells were fixed with 4% paraformaldehyde solution (Beyotime P0099) and stained with 0.1% crystal violet solution (Biosharp BL802A). The nontransplanted cells in the upper chamber were wiped with cotton swabs. Cells were observed under a microscope (Nikon Ti−S) and photographed.

2.7. Statistical Methods. Data were statistically analyzed by using GraphPad Prism 8.0.2. One-way analysis of variance (ANOVA) was used for multigroup measurement data, and SNK analysis was used for intergroup comparisons. The measurement data were statistically described using the mean ± standard deviation (±SD). *$p < 0.05$ indicated a statistically significant difference.

3. RESULTS

3.1. Characterization of DT Fraction of *S. miltiorrhiza*. High-performance liquid chromatography (HPLC) analysis revealed the presence of four compounds: tanshinone IIA, tanshinone I, cryptotanshinone, and dihydrotanshinone. The retention times of these compounds were 32.8, 18.1, 16.7, and 10.2 min, while the concentrations were 318.847, 203.761, 329.169, and 137.408 μg/mL, respectively. The HPLC chromatogram is given in Figure 1. The chemical structures of these phytochemicals are shown in Figure 2.

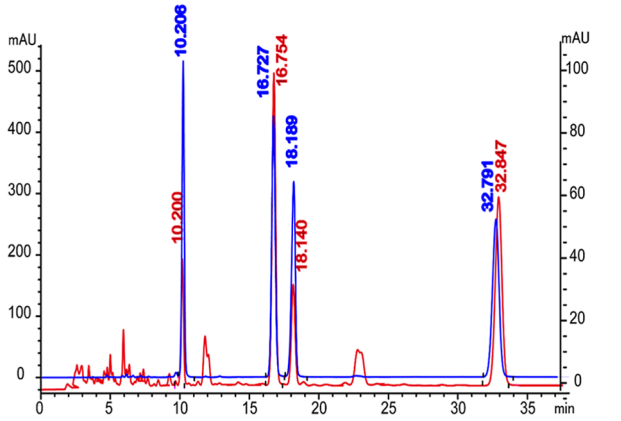

Figure 1. HPLC chromatogram of DT fraction extracted from *S. miltiorrhiza*; the red line indicates standard compound measurements, while the blue line indicates DT compound measurement.

3.2. DT Inhibited the Proliferation of the Lung Cancer Cell Line PC9. The efficacy of DT in treating tumors was first tested in vitro by incubating PC9 lung cancer cells with varying doses of DT (1, 1.5, 2, 2.5, 5, 10, 20, and 40 μg/mL) for 12 h. The results showed a reduction in cell proliferation in the PC9 lung cancer cell line, and the IC_{50} values of both the DT and PTX were comparable (as shown in Figure 3A). Additionally, the antitumor effects of DT (10 μg/mL) and DT (20 μg/mL) were compared with the standard drug paclitaxel (PTX; 10 μg/mL). DT (20 μg/mL) induced significant apoptosis in the lung cancer cell line compared to the control group. Similar findings were observed with PTX (10 μg/mL) treatment (as shown in

https://doi.org/10.1021/acsomega.3c09667
ACS Omega 2024, 9, 7230−7238

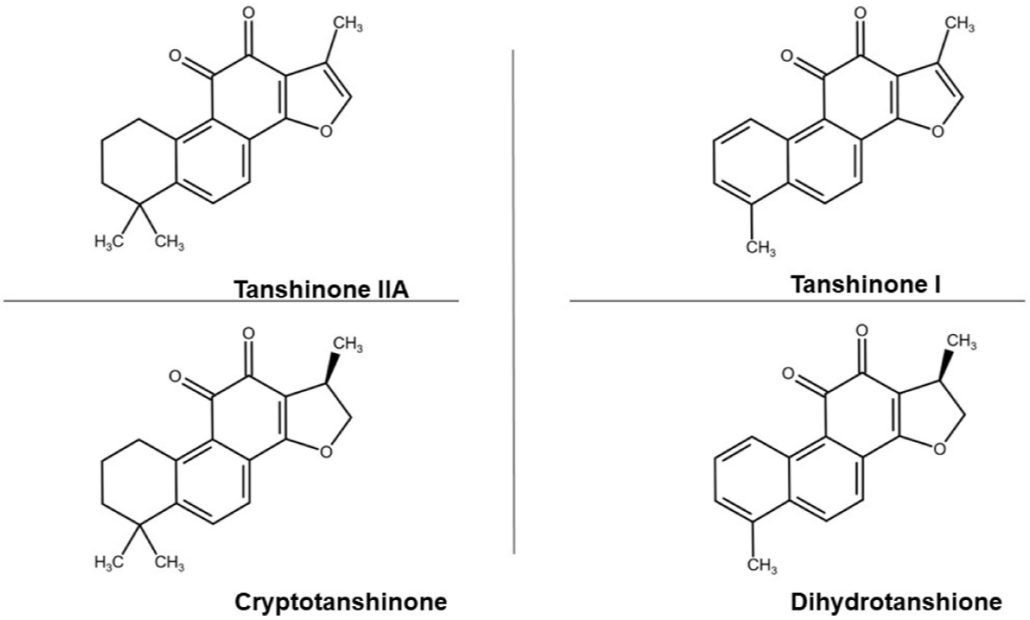

Figure 2. Phytochemical structures detected in the DT fraction.

Figure 3B). DT and PTX showed almost identical results. The wound-healing and trans well assays showed that both DT (at concentrations of 0, 2.5, and 5 μg/mL) and PTX (at a concentration of 1 μg/mL) promoted apoptosis and significantly inhibited the migration of PC9 cancer cells compared to cells without treatment (as shown in Figure 3C,D).

3.3. DT Inhibited the Tumor Growth in the BALB/C-NU Nude Mice. Observations were made regarding changes in tumor size over time, as measured by tumor volume and weight (Figure 4A,B). The tumor volume gradually increased from days 1 to 16. On the 16th day, different doses of DT fraction were administered, with PTX (60 mg/kg) being used as a standard chemotherapeutic drug. After 5 days of drug treatment, DT produced a significant dose-dependent effect. Increasing DT concentration resulted in a significant decrease in nude mice's tumor volume and weight (Figure 4B,C).

H&E staining of tumor tissue sections from the disease control group and all the treatment groups revealed that the cells from each treatment group had fewer nuclear and cell shape defects compared to the disease control group. As the DT concentration increased, the area of light pink and flaky necrotic regions within the PC9 transplant tumor increased (Figure 4D). The morphology of the necrotic areas within the tumor tissue of nude mice in the PTX administration groups was indifferent to the DT groups, with the necrotic areas surrounding their tumor cells forming a nested pattern.

3.4. DT Improved the Inflammatory TME in BALB/C-NU Nude Mice. Various types of inflammatory cells are infiltrated into tumor tissues and the degree of their infiltration determines the progress and efficacy of anticancer therapy.[30,31] We utilized IHC to detect CD31 and CD68 infiltration in PC9-induced solid lung tumors. CD31 is a platelet endothelial cell adhesion molecule-1 that is expressed on the surface of macrophages.[32,33] Vascular endothelial cells and platelets and showed a brownish-yellow granular or lamellar dark staining pattern (Figure 5A,B). CD68 is a TAM marker, and hence CD68 expression showed TAM infiltration in tumor tissues. CD68 expression was mainly located on the cell membrane, while a small amount was expressed in the intercellular stroma. CD68 IHC staining showed a brownish-yellow granular or sheet-like deep pattern. The results revealed that both CD31 and CD68 were expressed in tumor tissue, and this expression is an indication of inflammatory cell infiltration in the tumor tissue of BALB/c-nu mice. Treatment with increasing concentrations of DT significantly reduced the expression of CD31 and CD68, indicating a decrease in inflammatory cell infiltration.

3.5. DT Inhibited NF-κB p65 Expression in Lung Cancer Cells. Previous research has highlighted the crucial role played by NF-κB in both innate and adaptive immune responses.[34] It acts as a central coordinator and is responsible for controlling communication between cancer cells and inflammatory cells. Our study findings showed that there was a significant reduction in the expression of NF-κB p65 in the tumor tissue of the group administered with DT as compared to the control group (as shown in Figure 6A). PTX also had a similar effect. The tumor inflammatory microenvironment comprises a high density of inflammatory cell subsets. DT drug intervention has been found to significantly reduce the level of infiltration of inflammatory cells. This might happen due to reduced LPS paracellular transport that is depicted by the administration of DT resulting in a significant reduction in the level of LPS in the serum (as shown in Figure 6B). This led to the exploration of whether circulating LPS resulting from intestinal barrier dysfunction plays a role in DT treatment effects.

3.6. DT Improved Intestinal Integrity. Intestinal mucosal damage led to the elevated level of LPS in the blood.[35] However, the control, DT 60 mg/kg, and PTX groups were found to significantly improve intestinal integrity, as shown by H&E staining (Figure 7A). Laser scanning fluorescent microscopy demonstrated that DT treatment increased the expression level of key structural proteins, occludin 1 and ZO-1 (Figure 7B,C). Transmission electron microscopy (TEM) revealed that intestinal epithelial cells of the BALB/c-nu nude mouse control had swollen mitochondria, deformed spines, or even disappeared entirely (red

https://doi.org/10.1021/acsomega.3c09667
ACS Omega 2024, 9, 7230−7238

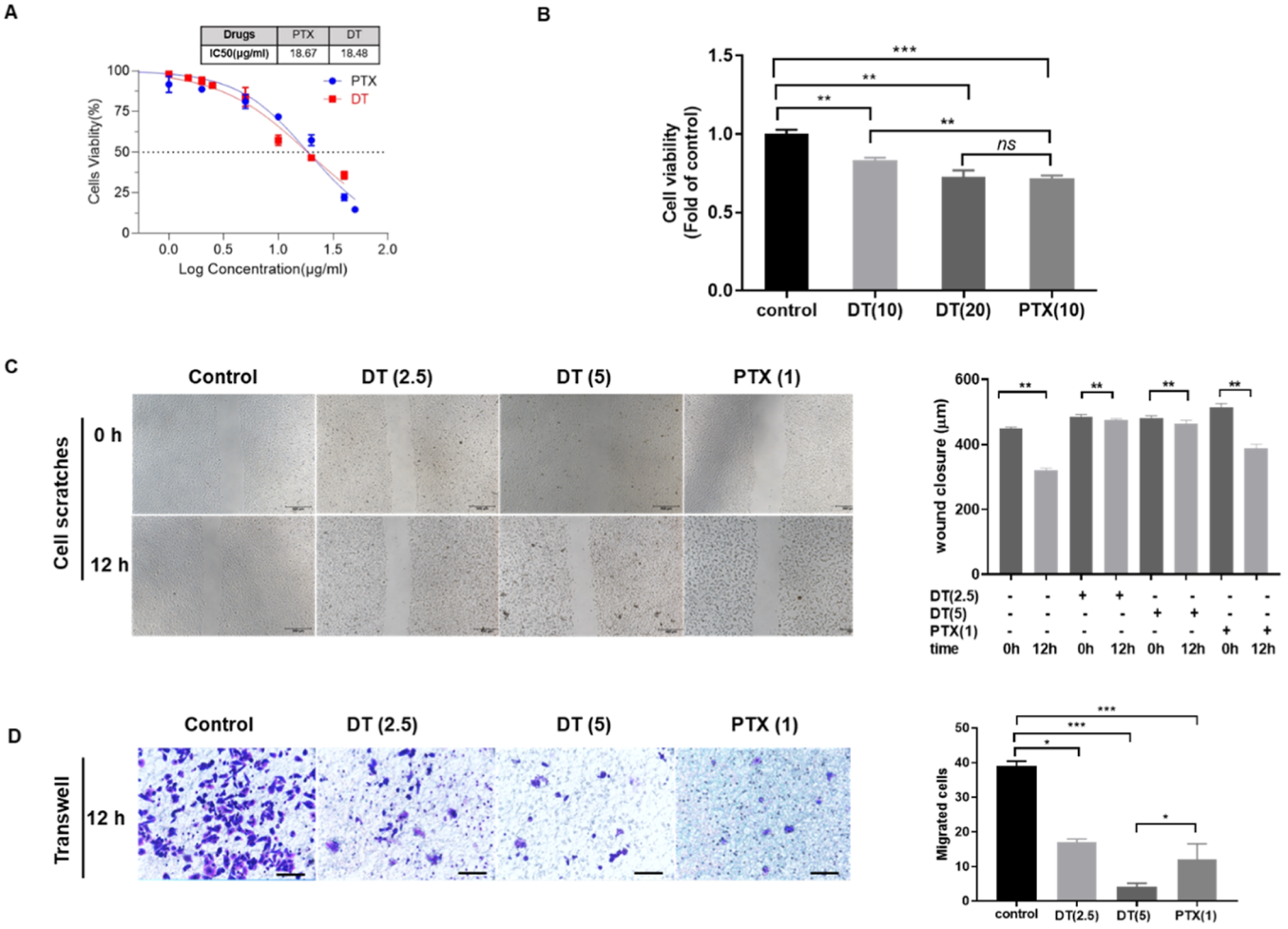

Figure 3. DT inhibited proliferation and induced apoptosis of the lung cancer cell line PC9. (A) Cell viability was assessed using the CCK-8 assay. (B) Cell viability after 12 h of DT (0, 10, and 20 μg/mL) and paclitaxel (PTX) (10 μg/mL) treatment. The number of surviving cells is expressed as the percentage of the control. (C) Representative results for PC9 cell scratch experiments after treatment: control, DT- (2.5 and 5 μg/mL), and PTX (1 μg/mL) for 12 h. (D) Representative results for the PC9 cell trans well assay after treatment: control, DT (2.5 and 5 μg/mL), and PTX (1 μg/mL). Data was analyzed statistically by using one-way ANOVA and multiple comparisons were performed by Tukey's post-hoc test. Results are considered significant if $^{*}p < 0.05$, $^{**}p < 0.01$, $^{***}p < 0.01$, and nonsignificant (ns) if $p > 0.05$; scale bar was 50 μM.

arrows) compared with the standard group (Figure 7D). As the concentration of DT increased, the mitochondrial structure in the intestinal epithelial cells of tumor-bearing nude mice gradually improved. Moreover, the extent of microvilli damage on the surface of these cells decreased, and there was a reduction in the size of cell gaps (white arrows). These results suggest that DT can rescue intestinal structural damage and maintain intestinal homeostasis.

4. DISCUSSION

Previous studies have shown that *S. miltiorrhiza* has potential anti-inflammatory and antitumor properties.[36] A DT-rich fraction was isolated from *S. miltiorrhiza*[37] and analyzed through HPLC to reveal the presence of tanshinone IIA, tanshinone I, cryptotanshinone, and dihydrotanshinone (Figures 1 and 2). All of these are anthraquinone derivatives. The results of this study demonstrated that the DT fraction inhibited PC9 lung cancer cell proliferation and growth in a dose-dependent manner. Moreover, Like paclitaxel, a standard chemotherapeutic agent, DT induced the apoptosis of lung cancer cells. IC_{50} values of both DT and PTX were calculated, and the results were comparable. To determine the inhibitory action of DT on the migration of PC9 cells, cell scratch wound-healing experiments and trans well assays were assessed. Our findings revealed that DT demonstrated a dose-dependent inhibition of both wound closure and the number of migrated cells, like the pattern observed with PTX. This suggests that DT may exert a similar inhibitory action on cell migration as PTX (Figure 3).

Lung tumors were induced in BALB/c-nu nude mice by subcutaneously injecting PC9 cells. Tumor growth was confirmed between days 1 and 16. The effects of DT treatment on tumor volume and weight were observed and found to be significantly detrimental, comparable to PTX. In addition, tissue histology and morphology were examined after H&E staining. DT treatment resulted in decreased cell shape defects and increased necrotic regions within PC9 cells, which appeared light pink and flaky. PTX also increased the necrotic area in tumor cells but with a nested appearance (Figure 4). Both results discussed above consistently showed that DT treatment not only induces apoptosis but also decreases tumor volume and weight as well as inhibits cell migration. PTX demonstrated similar effects. These antitumor effects of DT are consistent with previous findings (Figure 4).

https://doi.org/10.1021/acsomega.3c09667
ACS Omega 2024, 9, 7230−7238

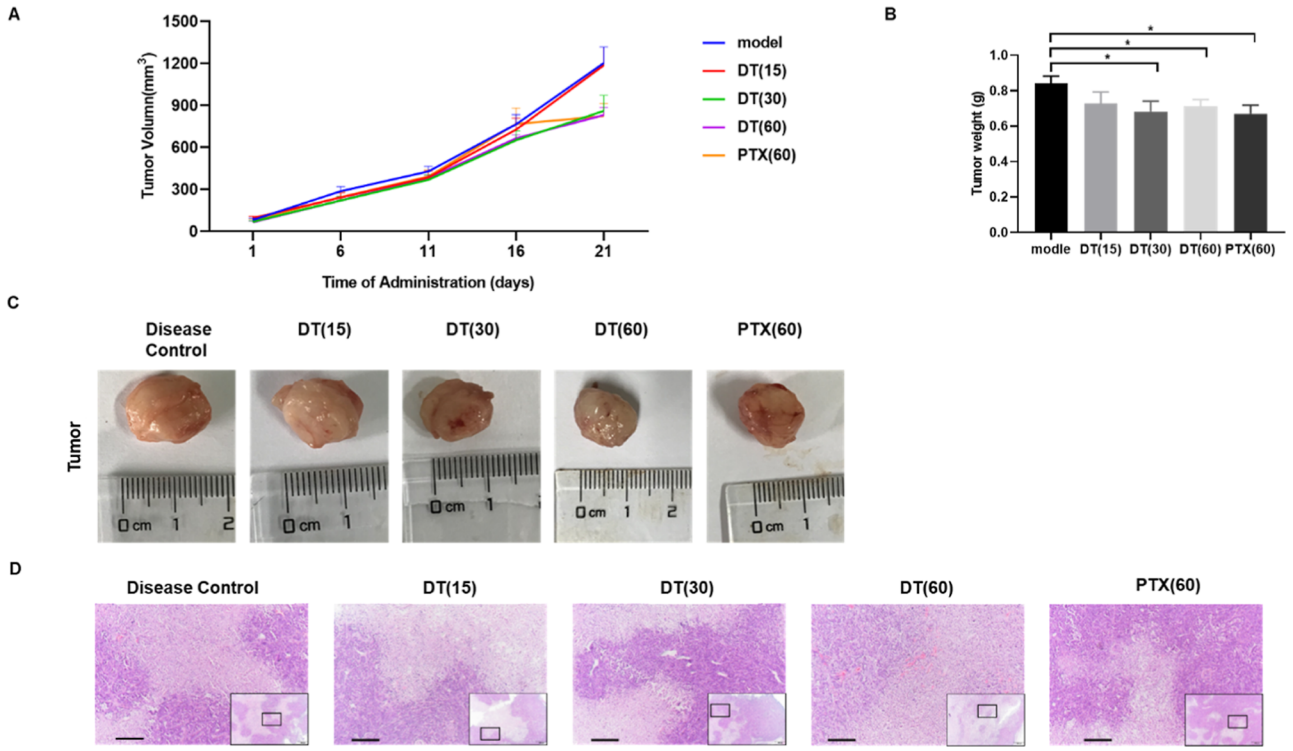

Figure 4. Effect of DT (15, 30, and 60 mg/kg) and PTX 60 mg/kg inhibited tumor growth in BALB/C-NU nude mice. (A) Changes in tumor diameter after drug administration. (B) Changes in tumor weight in each group after drug administration. (C) Changes in tumor size in each group after drug treatment. (D) H&E staining of the tumor tissue. DT (15, 30, and 60 mg/kg) and paclitaxel (PTX 60 mg/kg), depicting morphological changes in tumor tissues. DT showed a light pink and flaky necrotic region while PTX exhibited a necrotic region with a nested appearance. The scale bar was 100 μM.

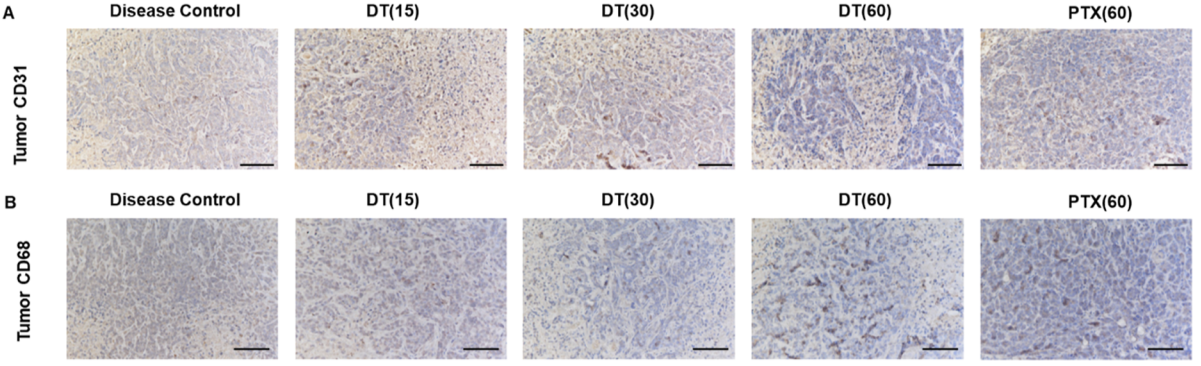

Figure 5. DT improved the inflammatory microenvironment in BALB/C-NU tumor nude mice. (A) IHC detection of CD31. Its expression showed a brownish-yellow granular or lamellar dark staining pattern in the control group, while CD31 expression was reduced with the treatment of DT in a dose-dependent manner as well as with PTX. (B) IHC detection of CD68 showed a brownish-yellow granular or sheet-like deep pattern. DT in a dose dose-dependent manner reduced the expression of CD68 and a similar pattern was observed with PTX. DT (15, 30, 60 mg/kg) and paclitaxel (PTX 60 mg/kg). The scale bar was 100 μM.

Previous research has made it clear that CD31 is a platelet endothelial cell adhesion molecule (PECAM-1). CD31 is a well-known marker of endothelial cells and plays a crucial role in the adhesion and accumulation of platelets. Its presence is also essential in cell proliferation, apoptosis, migration, and cellular immunity. On the other hand, CD68 is a TAM marker. Its higher expression is an indication of high vascularity and tumor metastasis.[33] In our study, we performed IHC staining and observed that CD31 expression showed a brownish-yellow granular or lamellar dark staining pattern, while CD68 expression showed a brownish-yellow granular or sheet-like deep appearance. The study findings indicate that all doses of DT significantly reduced the expression of both CD31 and CD68, in a dose-dependent manner, as shown in Figure 5 IHC staining pictures (Figure 5).

Anthraquinones found in natural drugs, such as in DT, have been reported to impact the inflammatory microenvironment through the NF-κB inflammatory signaling pathway.[38] This pathway also suppresses cancer.[39,40] NF-κB is a functional state of a protein that plays a key role in regulating the body's inflammatory response by entering the nucleus. Once inside the nucleus, it interacts with specific response elements on DNA and triggers the expression of various inflammatory genes. Elevated levels of LPS derived from gut bacteria in the

https://doi.org/10.1021/acsomega.3c09667
ACS Omega 2024, 9, 7230−7238

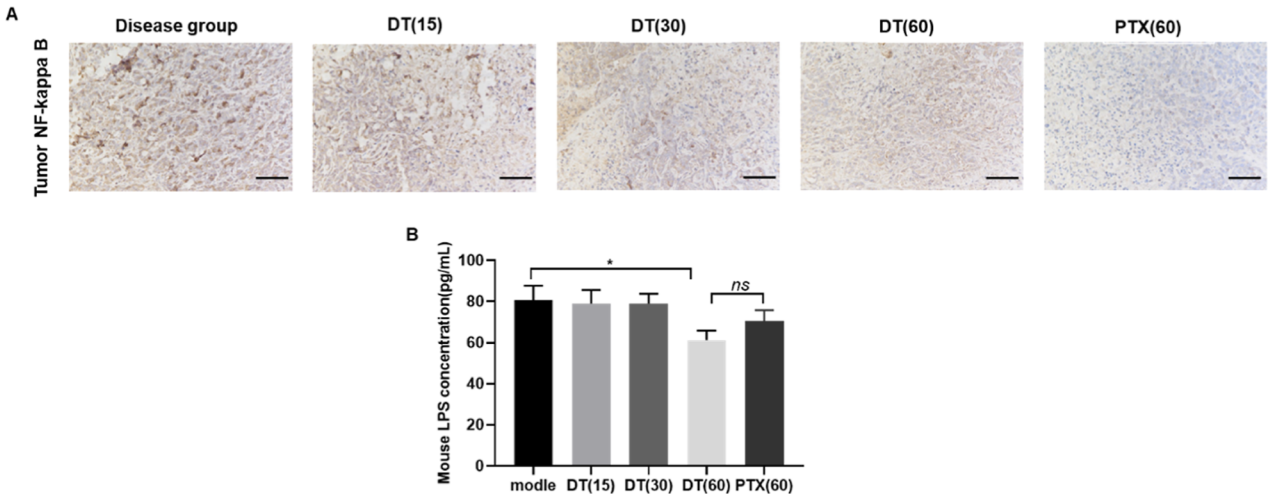

Figure 6. DT inhibited p65-NF-κB expression in lung cancer cells by decreasing the LPS level. (A) IHC detection of NF-κB expression in paraffin sections of solid tumor tissues. (B) LPS content in the serum of each group of mice. DT (15, 30, and 60 mg/kg) and paclitaxel (PTX 60 mg/kg). The scale bar was 100 μM.

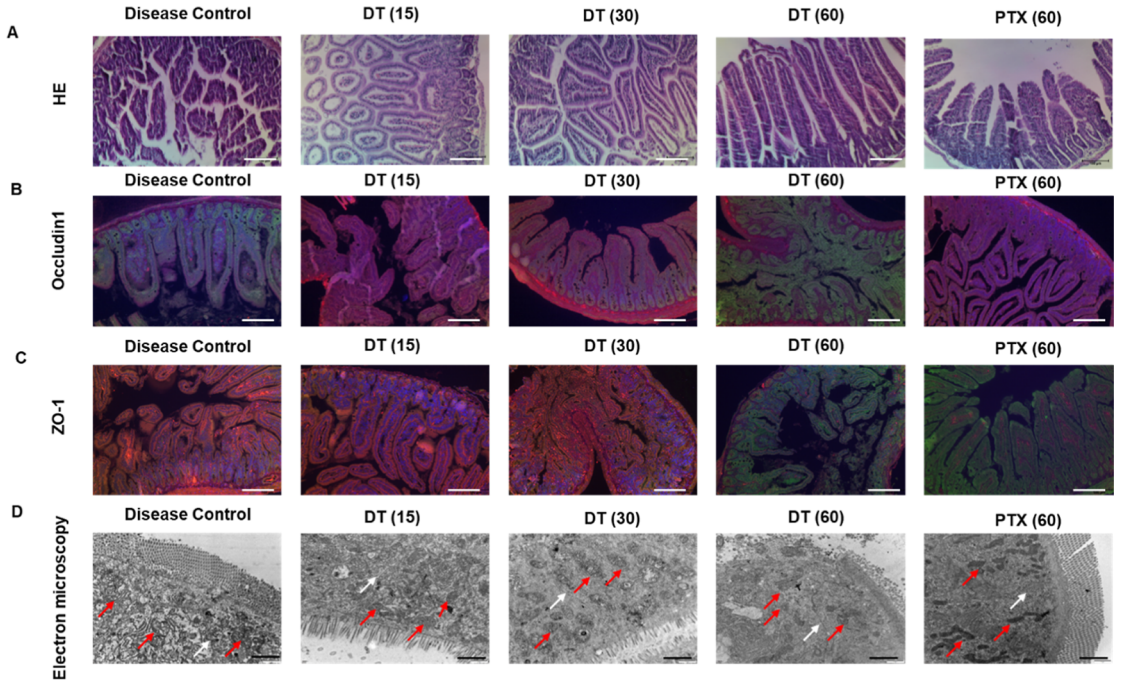

Figure 7. DT improves intestinal integrity by restoring mitochondrial function. (A) H&E stains for the intestinal tissue. (B) Laser scanning fluorescent microscopy of the intestinal tight junction proteins occludin 1 in various groups of BALB/C nude mice after drug intervention. Occludin 1 was labeled by Alexa Fluor 488 green fluorescence. Red fluorescence represented intestinal cell microfilament and was labeled Rhodamine's Phalloidin. Blue fluorescence (DAPI) represents the intestinal cell nucleus. (C) Laser scanning fluorescent microscopy of the intestinal tight junction proteins ZO-1 in various groups of BALB/C nude mice after drug intervention. ZO-1 was labeled by Alexa Fluor 488 green fluorescence. Red fluorescence represented intestinal cell microfilament and was labeled Rhodamine's Phalloidin. Blue fluorescence (DAPI) represents the intestinal cell nucleus. (D) TEM of the intestine of BALB/C nude mice in each group after drug intervention. The red arrow points to the mitochondria, and the white arrow points to the intercellular space. The scale bar was 100 μM for Figure A–C and 1 μM for Figure D.

blood are often caused by a breakdown in the intestinal barrier.[41,42] LPS acts as an exogenous endotoxin that is transported in the blood by lipoproteins or LPS-binding proteins, and it interacts with toll-like receptor 4 (TLR4) on the surface of immune cells, initiating the inflammatory response.[43,44] This triggers a signaling cascade that ultimately leads to increased expression of NF-κB and its associated proinflammatory cytokines.[45] This subset of inflammatory mediators aggravates tumor progression in the TME. Our study findings not only reduced the NF-κB expression but also reduced the LPS level in the blood, thus improving the TME (Figure 6).

The tight junction proteins ZO-1 and occludin I play a crucial role in maintaining the integrity of the intestines by preventing the paracellular transport of LPS into the bloodstream.[46] After DT treatment, the expression of ZO-1 and occludin 1 significantly increased, as shown by the H&E staining of tumor tissues extracted from BALB/C nude mice.

https://doi.org/10.1021/acsomega.3c09667
ACS Omega 2024, 9, 7230–7238

TEM images also showed the improvement in the expression of ZO-1 and occludin 1 which is evident with better mitochondria morphology and more presence of tight junction proteins, reduced swelling, and decreased deformed spines caused by subcutaneous tumors (Figure 7).

5. CONCLUSIONS

The study showed that DT-induced apoptosis in PC9 lung cancer cells reduced cell viability and inhibited cell migration. Furthermore, it reduced the lung tumor volume, weight, and size. The study also proved that DT improves the TME by reducing the levels of expression of CD31 and CD68. The molecular mechanism behind the tumor-suppressing ability of DT is related not only to direct apoptosis induction of tumor cells but also to upregulation of the expression of endothelial barrier tight junction proteins ZO-1 and occludin 1. These proteins might maintain intestinal integrity and reduce blood LPS levels, which interfere with TLR4-induced NF-κB expression. Therefore, it can be inferred that lung cancer progression could be stopped through the intestinal kidney inflammation axis. Further studies might provoke more precise mechanisms that could better unveil the role of intestinal integrity in improving the TME.

6. ETHICS APPROVAL AND INFORMED CONSENT

The animal study was reviewed and approved by the Animal Ethical and Welfare Committee of Zhejiang Chinese Medical University (institutional ethics approval number: IACUC-20200727-04). The study followed the guidelines outlined in the National Institutes of Health Guide for the Care and Use of Laboratory Animals.

AUTHOR INFORMATION

Corresponding Authors

Guangji Zhang − *College of Basic Medical Sciences, Zhejiang Chinese Medical University, Hangzhou 310053, P. R. China*; Email: zgj@zcmu.edu.cn

Liaqat Hussain − *Department of Pharmacology, Faculty of Pharmaceutical Science, Government College University, Faisalabad 38000, Pakistan*; orcid.org/0000-0001-7171-5917; Email: Liaqat.hussain@gcuf.edu.pk

Authors

Hao Xu − *College of Basic Medical Sciences, Zhejiang Chinese Medical University, Hangzhou 310053, P. R. China*

Ning Ning Guo − *Inner Mongolia Medical University, Hohhot 010110, P. R. China*

Chen Ying Zhu − *Department of Public Health, Zhejiang University School of Medicine, Hangzhou 310058, P. R. China*

Lin Yan Ye − *Department of Public Health, Zhejiang University School of Medicine, Hangzhou 310058, P. R. China*

Xing Yi Yan − *Department of Public Health, Zhejiang University School of Medicine, Hangzhou 310058, P. R. China*

Yong Qin Liu − *Department of Public Health, Zhejiang University School of Medicine, Hangzhou 310058, P. R. China*

Ze Yan Zhang − *Department of Public Health, Zhejiang University School of Medicine, Hangzhou 310058, P. R. China*

Complete contact information is available at: https://pubs.acs.org/10.1021/acsomega.3c09667

Author Contributions

⊥H.X. and N.N.G. contributed equally.

Notes

The authors declare no competing financial interest.

ACKNOWLEDGMENTS

The authors acknowledge the Zhejiang Provincial Science and Technology Program Project (2019C03072) and the State Key Program of the National Nature Science Foundation of China, grant number 82030119, for financial assistance.

REFERENCES

(1) *Cancer Statistics Lung Cancer Stat Bite*; US Department of Health and Human Services, 2023.

(2) *Lung Cancer—Non-Small Cell: Statistics*; American Society of Clinical Oncology, 2023. https://www.cancer.net/cancer-types/lung-cancer-non-small-cell/statistics.

(3) Hirsch, F. R.; Scagliotti, G. V.; Mulshine, J. L.; Kwon, R.; Curran, W. J.; Wu, Y.-L.; Paz-Ares, L. Lung cancer: current therapies and new targeted treatments. *Lancet* **2017**, *389* (10066), 299−311.

(4) Fu, L.; Han, B.; Zhou, Y.; Ren, J.; Cao, W.; Patel, G.; Kai, G.; Zhang, J. The anticancer properties of tanshinones and the pharmacological effects of their active ingredients. *Front. Pharmacol* **2020**, *11*, 193.

(5) Wu, C.-Y.; Yang, Y.-H.; Lin, Y.-S.; Chang, G.-H.; Tsai, M.-S.; Hsu, C.-M.; Yeh, R.-A.; Shu, L.-H.; Cheng, Y.-C.; Liu, H.-T. Dihydroisotanshinone I induced ferroptosis and apoptosis of lung cancer cells. *Biomed. Pharmacother.* **2021**, *139*, 111585.

(6) Li, Z.; Zhang, Y.; Zhou, Y.; Wang, F.; Yin, C.; Ding, L.; Zhang, S. Tanshinone IIA suppresses the progression of lung adenocarcinoma through regulating CCNA2-CDK2 complex and AURKA/PLK1 pathway. *Sci. Rep.* **2021**, *11* (1), 23681.

(7) Fan, Q.; Lu, Q.; Wang, G.; Zhu, W.; Teng, L.; Chen, W.; Bi, L. Optimizing component formula suppresses lung cancer by blocking DTL-mediated PDCD4 ubiquitination to regulate the MAPK/JNK pathway. *J. Ethnopharmacol.* **2022**, *299*, 115546.

(8) Bai, Y.; Zhang, L.; Fang, X.; Yang, Y. Tanshinone IIA enhances chemosensitivity of colon cancer cells by suppressing nuclear factor-κB. *Exp. Ther. Med.* **2016**, *11* (3), 1085−1089.

(9) Zhou, J.; Jiang, Y. y.; Chen, H.; Wu, Y. c.; Zhang, L. Tanshinone I attenuates the malignant biological properties of ovarian cancer by inducing apoptosis and autophagy via the inactivation of PI3K/AKT/mTOR pathway. *Cell Prolif.* **2020**, *53* (2), No. e12739.

(10) Chen, W.; Luo, Y.; Liu, L.; Zhou, H.; Xu, B.; Han, X.; Shen, T.; Liu, Z.; Lu, Y.; Huang, S. Cryptotanshinone inhibits cancer cell proliferation by suppressing mammalian target of rapamycin-mediated cyclin D1 expression and Rb phosphorylation. *Cancer Prev. Res.* **2010**, *3* (8), 1015−1025.

(11) Gao, R.; Wu, X.; Huang, Z.; Wang, B.; Li, F.; Xu, H.; Ran, L. Anti-tumor effect of aloe-emodin on cervical cancer cells was associated with human papillomavirus E6/E7 and glucose metabolism. *OncoTargets* **2019**, *12*, 3713−3721.

(12) Abu, N.; Zamberi, N. R.; Yeap, S. K.; Nordin, N.; Mohamad, N. E.; Romli, M. F.; Rasol, N. E.; Subramani, T.; Ismail, N. H.; Alitheen, N. B. Subchronic toxicity, immunoregulation and anti-breast tumor effect of Nordamnacantal, an anthraquinone extracted from the stems of Morinda citrifolia L. *BMC Complement Altern. Med.* **2018**, *18* (1), 31.

(13) Wang, T.; Zou, J.; Wu, Q.; Wang, R.; Yuan, C.-L.; Shu, J.; Zhai, B.-B.; Huang, X.-T.; Liu, N.-Z.; Hua, F.-Y.; et al. Tanshinone IIA derivatives induced S-phase arrest through stabilizing c-myc G-quadruplex DNA to regulate ROS-mediated PI3K/Akt/mTOR pathway. *Eur. J. Pharmacol.* **2021**, *912*, 174586.

(14) Liao, X. Z.; Gao, Y.; Huang, S.; Chen, Z. Z.; Sun, L. L.; Liu, J. H.; Chen, H. R.; Yu, L.; Zhang, J. X.; Lin, L. Z. Tanshinone IIA combined with cisplatin synergistically inhibits non-small-cell lung cancer in vitro and in vivo via down-regulating the phosphatidylinositol 3-kinase/Akt signalling pathway. *Phytother. Res.* **2019**, *33* (9), 2298−2309.
(15) Li, S.; Zhaohuan, L.; Guangshun, Z.; Guanhua, X.; Guangji, Z. Diterpenoid Tanshinones, the extract from Danshen (Radix Salviae Miltiorrhizae) induced apoptosis in nine human cancer cell lines. *Tradit. Chin. Med.* **2016**, *36* (4), 514−521.
(16) Lou, Z.-H.; Xia, R.-M.; Li, X.-J.; Cheng, R.-B.; Shao, K.-D.; Zhang, G.-J. Anti-lung cancer mechanisms of diterpenoid tanshinone via endoplasmic reticulum stress-mediated apoptosis signal pathway. *China J. Chin. Mater. Med.* **2018**, *43* (24), 4900−4907.
(17) Chen, Z.; Zhu, R.; Zheng, J.; Chen, C.; Huang, C.; Ma, J.; Xu, C.; Zhai, W.; Zheng, J. Cryptotanshinone inhibits proliferation yet induces apoptosis by suppressing STAT3 signals in renal cell carcinoma. *Oncotarget* **2017**, *8* (30), 50023−50033.
(18) Li, Y.; Gong, Y.; Li, L.; Abdolmaleky, H. M.; Zhou, J. R. J. M. c. Bioactive tanshinone I inhibits the growth of lung cancer in part via downregulation of Aurora A function. *Mol. Carcinog.* **2013**, *52* (7), 535−543.
(19) Balkwill, F. R.; Capasso, M.; Hagemann, T. The tumor microenvironment at a glance. *J. Cell Sci.* **2012**, *125* (23), 5591−5596.
(20) Yang, J.; Zhang, Z.; Chen, C.; Liu, Y.; Si, Q.; Chuang, T.; Li, N.; Gomez-Cabrero, A.; Reisfeld, R.; Xiang, R.; et al. MicroRNA-19a-3p inhibits breast cancer progression and metastasis by inducing macrophage polarization through downregulated expression of Fra-1 proto-oncogene. *Oncogene* **2014**, *33* (23), 3014−3023.
(21) Nasrollahzadeh, E.; Razi, S.; Keshavarz-Fathi, M.; Mazzone, M.; Rezaei, N. Pro-tumorigenic functions of macrophages at the primary, invasive and metastatic tumor site. *Cancer Immunol. Immunother.* **2020**, *69*, 1673−1697.
(22) Jaynes, J. M.; Sable, R.; Ronzetti, M.; Bautista, W.; Knotts, Z.; Abisoye-Ogunniyan, A.; Li, D.; Calvo, R.; Dashnyam, M.; Singh, A.; et al. Mannose receptor (CD206) activation in tumor-associated macrophages enhances adaptive and innate antitumor immune responses. *Sci. Transl. Med.* **2020**, *12* (530), No. eaax6337.
(23) Liu, L.; Guo, H.; Song, A.; Huang, J.; Zhang, Y.; Jin, S.; Li, S.; Zhang, L.; Yang, C.; Yang, P. J. B. i. Progranulin inhibits LPS-induced macrophage M1 polarization via NF-κB and MAPK pathways. *BMC Immunol.* **2020**, *21* (1), 32.
(24) Wang, Y.-M.; Ji, R.; Chen, W.-W.; Huang, S.-W.; Zheng, Y.-J.; Yang, Z.-T.; Qu, H.-P.; Chen, H.; Mao, E.-Q.; Chen, Y.; et al. Paclitaxel alleviated sepsis-induced acute lung injury by activating MUC1 and suppressing TLR-4/NF-κB pathway. *Drug Des. Dev. Ther.* **2019**, *13*, 3391−3404.
(25) Zheng, Y.; Zheng, M.; Shao, J.; Jiang, C.; Shen, J.; Tao, R.; Deng, Y.; Xu, Y.; Lu, Y. Upregulation of claudin-4 by Chinese traditional medicine Shenfu attenuates lung tissue damage by acute lung injury aggravated by acute gastrointestinal injury. *Pharm. Biol.* **2022**, *60* (1), 1981−1993.
(26) Garrett, W. S. Cancer and the microbiota. *Science* **2015**, *348* (6230), 80−86.
(27) Mao, Q.; Jiang, F.; Yin, R.; Wang, J.; Xia, W.; Dong, G.; Ma, W.; Yang, Y.; Xu, L.; Hu, J. Interplay between the lung microbiome and lung cancer. *Cancer Lett.* **2018**, *415*, 40−48.
(28) Li, M.; Zhang, R.; Li, J.; Li, J. The role of C-type lectin receptor signaling in the intestinal microbiota-inflammation-cancer axis. *Front. Immunol.* **2022**, *13*, 894445.
(29) Zhao, Y.; Liu, Y.; Li, S.; Peng, Z.; Liu, X.; Chen, J.; Zheng, X. Role of lung and gut microbiota on lung cancer pathogenesis. *J. Cancer Res. Clin. Oncol.* **2021**, *147* (8), 2177−2186.
(30) Solinas, G.; Germano, G.; Mantovani, A.; Allavena, P. Tumor-associated macrophages (TAM) as major players of the cancer-related inflammation. *J. Leukoc. Biol.* **2009**, *86* (5), 1065−1073.
(31) Greten, F. R.; Grivennikov, S. I. J. I. Inflammation and cancer: triggers, mechanisms, and consequences. *Immunity* **2019**, *51* (1), 27−41.
(32) Diana, A.; Wang, L. M.; D'Costa, Z.; Azad, A.; Silva, M. A.; Soonawalla, Z.; Allen, P.; Liu, S.; McKenna, W. G.; Muschel, R. J.; et al. Prognostic role and correlation of CA9, CD31, CD68 and CD20 with the desmoplastic stroma in pancreatic ductal adenocarcinoma. *Oncotarget* **2016**, *7* (45), 72819−72832.
(33) McKenney, J. K.; Weiss, S. W.; Folpe, A. L. CD31 expression in intratumoral macrophages: a potential diagnostic pitfall. *Am. J. Surg. Pathol.* **2001**, *25* (9), 1167−1173.
(34) Fan, Y.; Mao, R.; Yang, J. NF-κB and STAT3 signaling pathways collaboratively link inflammation to cancer. *Protein Cell* **2013**, *4*, 176−185.
(35) Wu, H.; Xie, S.; Miao, J.; Li, Y.; Wang, Z.; Wang, M.; Yu, Q. Lactobacillus reuteri maintains intestinal epithelial regeneration and repairs damaged intestinal mucosa. *Gut Microb.* **2020**, *11* (4), 997−1014.
(36) Shi, M.; Huang, F.; Deng, C.; Wang, Y.; Kai, G. Bioactivities, biosynthesis and biotechnological production of phenolic acids in Salvia miltiorrhiza. *Crit. Rev. Food Sci. Nutr.* **2019**, *59* (6), 953−964.
(37) Su, Y.-S.; Kuo, M. Z.; Kuo, Y. T.; Huang, S.-W.; Lee, C.-J.; Su, Z.-Y.; Ni, Y.-H.; Li, D.-K.; Wu, T.-Y. Diterpenoid anthraquinones as chemopreventive agents altered microRNA and transcriptome expressions in cancer cells. *Biomed. Pharmacother.* **2021**, *136*, 111260.
(38) Luo, R.; Lin, M.; Fu, C.; Zhang, J.; Chen, Q.; Zhang, C.; Shi, J.; Pu, X.; Dong, L.; Xu, H.; et al. Calcium pectinate and hyaluronic acid modified lactoferrin nanoparticles loaded rhein with dual-targeting for ulcerative colitis treatment. *Carbohydr. Polym.* **2021**, *263*, 117998.
(39) Du, Y.; Qian, B.; Gao, L.; Tan, P.; Chen, H.; Wang, A.; Zheng, T.; Pu, S.; Xia, X.; Fu, W. Aloin preconditioning attenuates hepatic ischemia/reperfusion injury via inhibiting TLR4/MyD88/NF-κB signal pathway in vivo and in vitro. *Oxid. Med. Cell. Longev.* **2019**, *2019*, 1−14.
(40) Chen, Q.; Luo, R.; Han, X.; Zhang, J.; He, Y.; Qi, S.; Pu, X.; Nie, W.; Dong, L.; Xu, H.; et al. Entrapment of macrophage-target nanoparticles by yeast microparticles for rhein delivery in ulcerative colitis treatment. *Biomacromolecules* **2021**, *22* (6), 2754−2767.
(41) Ciesielska, A.; Matyjek, M.; Kwiatkowska, K. TLR4 and CD14 trafficking and its influence on LPS-induced pro-inflammatory signaling. *Cell. Mol. Life Sci.* **2021**, *78*, 1233−1261.
(42) Fan, J.; Liu, S.; Ai, Z.; Chen, Y.; Wang, Y.; Li, Y.; Li, X.; Xiao, S.; Wang, Y. Fermented ginseng attenuates lipopolysaccharide-induced inflammatory responses by activating the TLR4/MAPK signaling pathway and remediating gut barrier. *Food Funct.* **2021**, *12* (2), 852−861.
(43) Liu, D.; Zhang, Y.; Liu, Y.; Hou, L.; Li, S.; Tian, H.; Zhao, T. Berberine modulates gut microbiota and reduces insulin resistance via the TLR4 signaling pathway. *Exp. Clin. Endocrinol. Diabetes* **2018**, *126* (08), 513−520.
(44) Chen, H.; Yang, H.; Deng, J.; Fan, D. Ginsenoside Rk3 ameliorates obesity-induced colitis by regulating of intestinal flora and the TLR4/NF-κB signaling pathway in C57BL/6 mice. *J. Agric. Food Chem.* **2021**, *69* (10), 3082−3093.
(45) Zhang, X.; Su, C.; Zhao, S.; Li, J.; Yu, F. Combination therapy of Ulinastatin with Thrombomodulin alleviates endotoxin (LPS)—induced liver and kidney injury via inhibiting apoptosis, oxidative stress and HMGB1/TLR4/NF-κB pathway. *Bioengineered* **2022**, *13* (2), 2951−2970.
(46) Cario, E.; Gerken, G.; Podolsky, D. K. Toll-like receptor 2 enhances ZO-1-associated intestinal epithelial barrier integrity via protein kinase C. *Gastroenterology* **2004**, *127* (1), 224−238.

https://doi.org/10.1021/acsomega.3c09667
ACS Omega 2024, 9, 7230−7238